

Merging Top-Down and Bottom-Up Approaches to Fabricate Artificial Photonic Nanomaterials with a Deterministic Electric and Magnetic Response

Kay Dietrich,* Matthias Zilk, Martin Steglich, Thomas Siefke,* Uwe Hübner, Thomas Pertsch, Carsten Rockstuhl, Andreas Tünnermann, and Ernst-Bernhard Kley

Artificial photonic nanomaterials made from densely packed scatterers are frequently realized either by top-down or bottom-up techniques. While top-down techniques offer unprecedented control over achievable geometries for the scatterers, by trend they suffer from being limited to planar and periodic structures. In contrast, materials fabricated with bottom-up techniques do not suffer from such disadvantages but, unfortunately, they offer only little control on achievable geometries for the scatterers. To overcome these limitations, a nanofabrication strategy is introduced that merges both approaches. A large number of scatterers are fabricated with a tailored optical response by fast character projection electron-beam lithography and are embedded into a membrane. By peeling-off this membrane from the substrate, scrambling, and densifying it, a bulk material comprising densely packed and randomly arranged scatterers is obtained. The fabrication of an isotropic material from these scatterers with a strong electric and magnetic response is demonstrated. The approach of this study unlocks novel opportunities to fabricate nanomaterials with a complex optical response in the bulk but also on top of arbitrarily shaped surfaces.

1. Introduction

Artificial photonic nanomaterials have been explored for a long time.^[1–3] They consist of strongly scattering nanostructures that are densely packed in space, such that the propagating light experiences on some effective scale a homogenous medium with properties inaccessible in nature.^[4] To go beyond the mere spatial average of the intrinsic properties of the constituents, the nanostructures are tailored to resonantly interact with light. For long time, small metallic nanoparticles have been considered, where thanks to the excitation of localized plasmon polaritons a strong electric dipolar response is induced at a resonance frequency.^[5] The research gained tremendous momentum in the past with the appreciation that nanostructures fashioned in a more complicated geometry can also offer a strong

magnetic dipolar response. In analogy to ordinary materials these nanostructures are frequently called meta-atoms.^[6] In perspective, this offers materials with a strong electric and magnetic response, which would unlock unprecedented application perspectives.^[7] The application perspectives would even widen by employing various mechanisms for tuning the optical response.^[8,9]

Initially, the necessary materials were fabricated with top-down approaches, such as electron beam-lithography or focused ion beam milling.^[10–13] Such techniques offer the benefit of a deterministic control on the accessible geometries. This was decisive to induce the desired response with a notable strength and not just as a small perturbation on top of a response offered by the background material.^[14,15] However, it comes with disadvantages. First, the accessible meta-atoms have been largely restricted to planar geometries and thin films. Second, the technologies are biased toward fabricating periodic arrangements that are the cause for artificial and detrimental effects. This concerns, e.g., the onset of lattice resonances, constituting a clear indication that the photonic nanomaterial is not homogenous. Also, the strong anisotropy is a clear disadvantage. To cause a disordered arrangement of the meta-atoms to suppress these effects, of course, is possible with top-down technologies, but the limitation to two-dimensional arrangements persists.^[16–18]


Dr. K. Dietrich, M. Zilk, Dr. M. Steglich, T. Siefke, Prof. T. Pertsch, Prof. A. Tünnermann, Dr. E.-B. Kley
Institute of Applied Physics
Abbe Center of Photonics
Friedrich-Schiller-Universität Jena
07743 Jena, Germany
E-mail: kay.dietrich@leibniz-ipht.de; thomas.siefke@uni-jena.de

Dr. U. Hübner
Leibniz Institute of Photonic Technology
07702 Jena, Germany

Prof. T. Pertsch, Prof. A. Tünnermann
Fraunhofer Institute for Applied Optics and Precision Engineering
07745 Jena, Germany

Prof. C. Rockstuhl
Institute of Theoretical Solid State Physics
Karlsruhe Institute of Technology
76131 Karlsruhe, Germany

Prof. C. Rockstuhl
Institute of Nanotechnology
Karlsruhe Institute of Technology
76021 Karlsruhe, Germany

 The ORCID identification number(s) for the author(s) of this article can be found under <https://doi.org/10.1002/adfm.201905722>.

© 2019 The Authors. Published by WILEY-VCH Verlag GmbH & Co. KGaA, Weinheim. This is an open access article under the terms of the Creative Commons Attribution License, which permits use, distribution and reproduction in any medium, provided the original work is properly cited.

DOI: 10.1002/adfm.201905722

To remedy these limitations, bottom-up techniques that mostly rely on self-assembly strategies have been considered.^[19–21] Thanks to the disordered and amorphous arrangement of the meta-atoms, isotropic and bulk nanomaterials are easily in reach.^[22–24] Also, large-scale fabrication techniques for planar metasurfaces have been reported where the constituents are brought afterward in solution after dissolving the particles.^[25,26] However, the approach remained so far limited as the building blocks are mostly small spherical nanoparticles, nanorods, or crescents that, even though combined in complex patterns, do not give the necessary degrees of freedom to tailor any desired response.^[27,28] Also, the density at which the meta-atoms can be arranged is rather low and often insufficient to induce a strong response in the bulk material.^[29]

2. Fundamental Concept

To make the best out of the two worlds, we introduce and demonstrate a fabrication route that merges top-down and bottom-up approaches, as illustrated in **Figure 1**. We start by fabricating with a high-speed and large-scale electron beam lithography^[30] process complicated but spatially quite homogenous^[31] strongly scattering meta-atoms on top of a thin sacrificial layer on a substrate. Here, we choose a metal-dielectric-metal meta-atom that sustains a strong electric and magnetic dipolar resonance. The realization of the meta-atom is schematically sketched in **Figure 1a** with a cross-sectional view at four instances during fabrication. Please note, the length scales in these figures are not to scale. The exact geometrical dimensions can be extracted later from the text. The four fabrication steps are briefly summarized in the following. The initial layer stack comprised a fused silica substrate (FS), a thin sacrificial layer (AZ), and a double layer of electron beam resist (CSAR and ARP). The resist stack was exposed by electron beam lithography in cell projection mode^[33] with a circular pattern arranged in a square periodic fashion and afterward developed. Thereafter, subsequently Au, SiO₂, and Au were deposited. Finally, the residual material was removed by lift-off. The meta-atoms are integrated into a membrane by spin-coating a thin layer of polyvinyl alcohol (PVA)

(**Figure 1b**) in which they continue to be embedded after the sacrificial layer is selectively dissolved and thus releasing the membrane from the substrate (**Figure 1c**). The membrane can be scrambled, to introduce the necessary disorder (**Figure 1d**), and densified (**Figure 1e**), to make a bulk material out of it that can be deposited at any desired surface. We chose a planar substrate and achieve with that a thick material layer that inherits its optical response from the individual meta-atoms (**Figure 1f**). Thanks to the random arrangement and orientation of the meta-atoms, the optical response is isotropic. More details are discussed in the Experimental Section.

3. Results and Discussion

3.1. Specification of the Meta-Atom Design

To start with, we design a meta-atom that offers simultaneously a strong electric dipolar resonance (EDR) and a magnetic dipolar resonance (MDR). As an appropriate meta-atom, a circular shaped cut-wire pair was designed comprising two layers of gold (Au) separated by a thin dielectric silica (SiO₂) spacer. This design, sketched in **Figure 2a**, allows to optically excite both the EDR and MDR that are characterized by a symmetric and antisymmetric current distribution.^[32] To confirm the excitability of both resonances, numerical simulations were performed with a modeled meta-atom diameter of $D = 160$ nm and layer thicknesses of $T_{\text{Au}} = 30$ nm and $T_{\text{SiO}_2} = 20$ nm. The meta-atom was embedded in a lossless dielectric host medium here assumed with a constant index of refraction of 1.5. The light was incident on the nanostructure array along the z -direction and both the transmitted power spectrum and the electric field vector in the vicinity of the meta-atom were recorded. **Figure 2b** shows slices of the magnitude (color map) and in overlay the direction (stream map) of the normalized electric field at $x = 0$. As noticeable by the symmetry of the stream map, each resonance can be associated of either being an EDR or MDR. The diagram in **Figure 2c** shows the extinction, which is the sum of absorption and scattering, as a function of the excitation

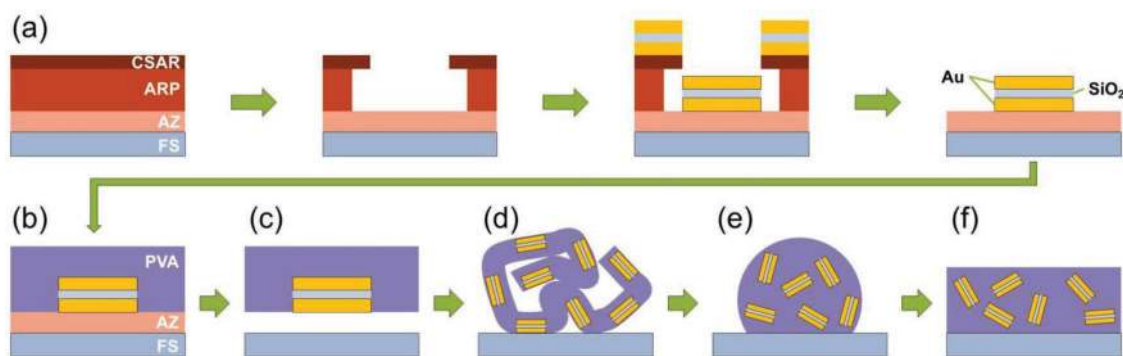


Figure 1. Schematic sketchings of the applied process chain for a) realizing the deterministic meta-atoms and b–f) reorienting and rearranging the meta-atoms toward an artificial 3D photonic nanomaterial. Please note, geometric dimensions in this figure are not to scale. a) A meta-atom array is realized by consecutively spin-coating, applying electron beam lithography in cell projection mode, developing, thermal evaporating an Au–SiO₂–Au layer stack and lift-off. The isotropic nanomaterial is realized by b) embedding the meta-atoms via spin-coating, c) selectively dissolving the sacrificial layer, d) dry-blowing and densifying, e) dissolving, and f) reshaping the meta-atom membrane cluster. Abbreviations are as follows: CSAR/ARP, electron beam resists; AZ, sacrificial layer; FS, substrate; Au, gold; SiO₂, silica; PVA, membrane.

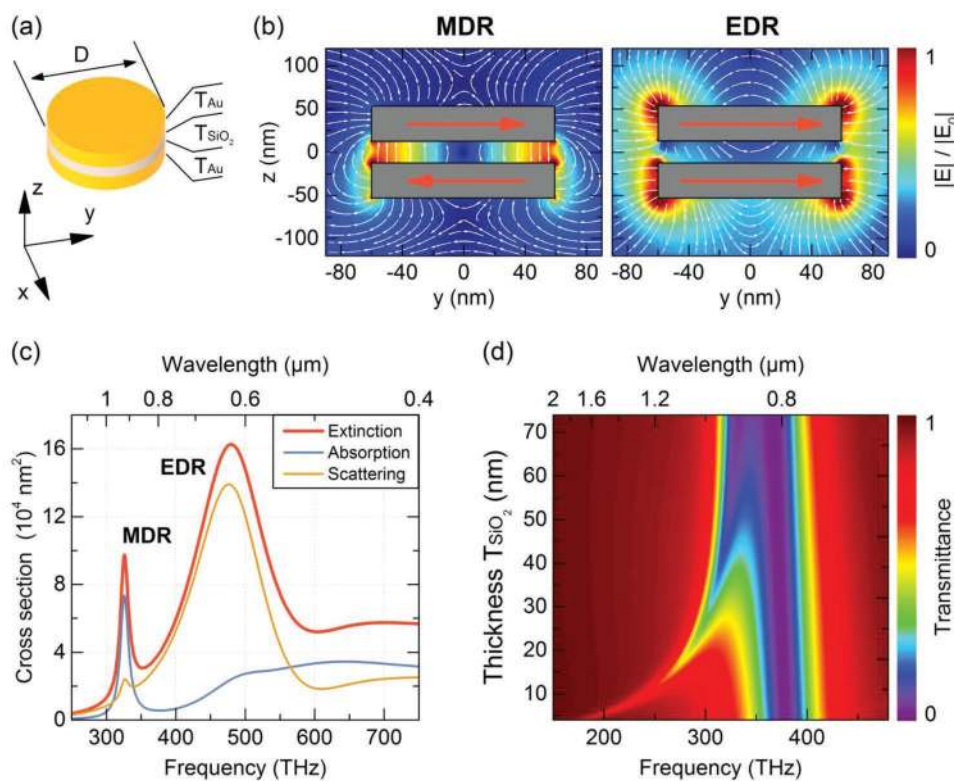


Figure 2. a) Sketch of the designed meta-atom with diameter D and thicknesses T of the respective material layers. b) Calculated electric field magnitude (color map) and field direction (stream map) in the vicinity of the meta-atom at both excited resonances (MDR: magnetic and EDR: electric dipole resonance). c) Calculated extinction spectrum of a single meta-atom with $T_{SiO_2} = 20$ nm and d) dependence of transmittance of a meta-atom array on excitation frequency and thickness of the dielectric silica spacer T_{SiO_2} . In (c) and (d) the meta-atom was modeled with $D = 160$ nm and $T_{Au} = 30$ nm.

frequency (wavelength). It is notably visible that the extinction cross section features two distinct maxima at either 325 THz or 480 THz. Both extinction maxima are related to the excited EDR and MDR shown in Figure 2b.

In order to tune both resonances, the geometrical parameters can be modified. While changing the thickness of both metallic layers or the diameter of the overall meta-atom equivalently shifts both resonances (not shown), changing the dielectric spacer thickness has an influence mostly on the MDR as shown in the color map of Figure 2d. In this analysis we consider in addition instead of the scattering cross section the transmission through an array of such particles, as it also corresponds to the situation accessible in the later experiment. It can be clearly seen, that the resonances translate into well-defined dips in the transmittance spectrum. At small spacer thicknesses both resonances are well separated in frequency. With increasing spacer thickness, the MDR shifts toward the EDR. Meanwhile the EDR remains almost unaffected in excitation frequency and thus the overlap of both resonances increases. For the experiment we will chose a thickness of 8 nm for the dielectric spacer to have resonances that are spectrally well separated.

3.2. Realization of the Meta-Atom Array

A photograph of the yielded meta-atom array (refer to last instance of Figure 1a) on a large-scale circular substrate

(diameter of 100 mm) is shown in Figure 3a. The central area with a total diameter of 70 mm contains the meta-atom array. The outer yellowish ring arose due to fabrication aspects and is not of further interest. A closer morphological investigation of the nanostructure was done by scanning electron microscopy (SEM). Figure 3b shows a tilted and cross-sectional view of the meta-atoms and confirms the separation of both metallic Au layers by the dielectric SiO₂ spacer (see the inset). Instead of a straight cylindrical wall, a more conical shape of the meta-atom is visible. The taper stems from the degradation of the resist mask during evaporation. According to the micrographs a taper angle of 10 degrees, a meta-atom diameter at the bottom of 140 nm, a thickness of each Au layer of 30 nm and a thickness of the SiO₂ layer of 8 nm were measured. After characterization of the meta-atom's geometry the sample was further prepared by spin-coating a thin layer of ≈ 500 nm PVA fully covering the meta-atoms as it has been schematically sketched in Figure 1b. This prepared the sample for subsequent optical characterization by ensuring a homogeneous optical embedding of the meta-atoms in the surrounding material.

3.3. Optical Investigation of the Meta-Atom Array

Optical transmittance spectroscopy was performed to confirm the optical functionality and the homogeneity of the entire nanostructured surface. Therefore, the sample was illuminated

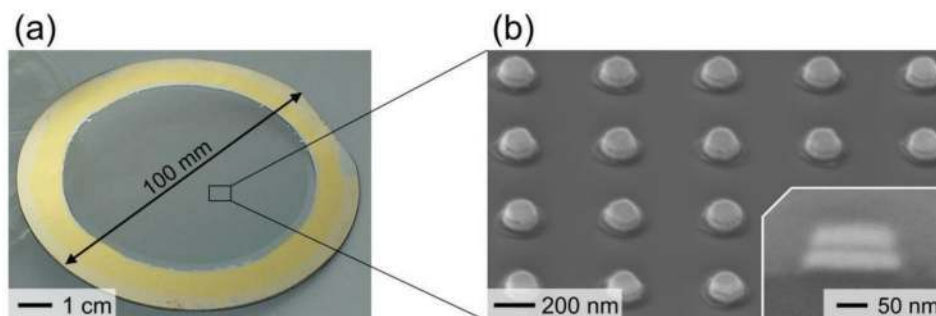


Figure 3. a) Photograph of the substrate carrying the meta-atom array (inner gray part) surrounded by a gold ring. b) Close-up tilted and cross-sectional (inset) view of the meta-atoms taken by SEM.

by perpendicularly incident light with a spot diameter of 2 mm. The spot was scanned over the sample, while after each measurement the sample was laterally shifted by a distance of 4 mm. In total 240 spectra were obtained. **Figure 4a** displays the median spectrum of all spectra (red line) normalized against air. In the diagram included are the $Q_{0.1}$ and $Q_{0.9}$ deciles (black lines) and a spectrum obtained by numerical simulation (blue line) with a nanostructure modeled according to the morphological results revealed by the close-up SEM images (see **Figure 3b**). The simulated result matches adequately with the median spectrum, as both dipole resonances are observable and the spectral locations coincide. Deviations mainly originate from morphological variations, which might be structure diameter, individual layer thicknesses, taper angle and an asymmetrical shape. For example, on one hand a certain structure diameter variation spectrally broadens and lifts the transmittance drop as perceptible at the EDR. On the other hand, a certain layer thickness increase of all three layers broadens and drops the transmittance as noticeable at the MDR.

To figure out the origin of the variations in the optical response over the entire wafer, both resonances of each of the 240 spectra were fitted independently with a Lorentz function in terms of resonance frequency position $\omega_0^{\text{MDR/EDR}}$, full width at half minimum $\gamma^{\text{MDR/EDR}}$, and amplitude $A^{\text{MDR/EDR}}$.

Figure 4b shows their dependence on the lateral sample position x and y in the respective heat map, while mainly two distribution patterns are visible. The first is a dominantly ring-like distribution excellently visible by $\omega_0^{\text{MDR/EDR}}(x,y)$. This is probably caused by a change of the proximity effect^[34] at the outer edge of the wafer resulting in a locally lower exposure dose respectively a smaller diameter of the meta-atom. The second is a variation across the wafer from the upper left to the lower right well noticeable by $A^{\text{MDR/EDR}}(x,y)$. This appearance is most likely induced by an off-centered wafer position during deposition paired with respect to the point-like evaporation source. This provokes a tilted projection coating resulting in an asymmetrical meta-atom shape. Nonetheless, the morphological variations are small across the entire wafer. Therefore, it is expected that the optical response of a random fraction of all meta-atoms will further on indicate all specific features in the transmission spectrum, as suggested by the median spectrum shown in **Figure 4a**.

3.4. Reshaping toward Photonic Nanomaterial

With the optical and morphological characteristics of the single layer of meta-atoms at hand, reorientation and rearrangement

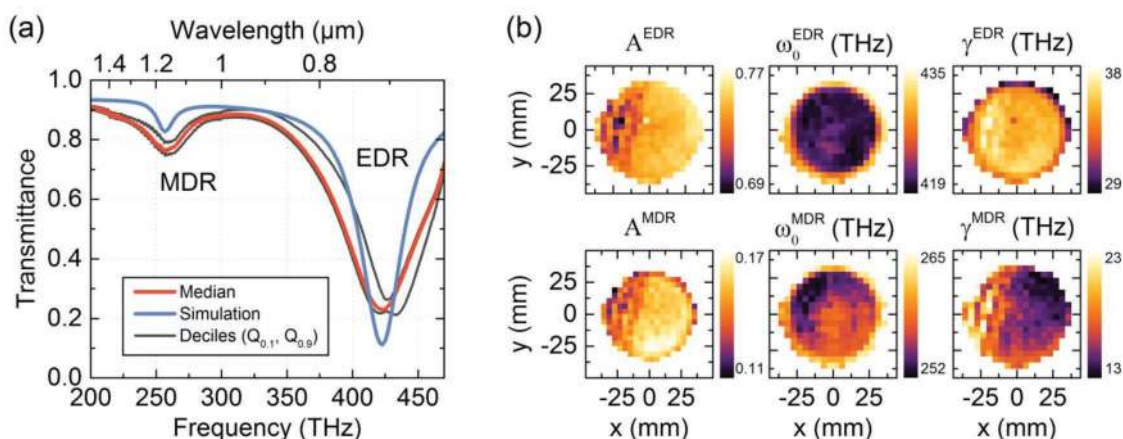


Figure 4. a) Median spectrum (red line), the deciles $Q_{0.1}$ and $Q_{0.9}$ (black lines) and for comparison a numerically simulated spectrum (blue line) in transmittance. b) Spatially resolved amplitude value, frequency position, and full width at half minimum (from left to right) after fitting the EDR (upper row) and MDR (lower row).

of all meta-atoms were initiated. Therefore, the 500 nm thick PVA layer with embedded meta-atoms was peeled-off the substrate by selectively removing the underlying sacrificial layer and thus turning the embedded meta-atom layer into a transferable and optically functionalized membrane. PVA is purely soluble in water. While the sacrificial layer is soluble in acetone-based solutions the PVA layer remains intact and keeps the meta-atoms firmly gripped. Although the PVA layer is extremely thin, it remains highly flexible and crack-free. This can be seen in the photograph in **Figure 5a** showing the membrane floating in a liquid after peel-off. As the multicolored iridescence hints, the meta-atoms are embedded in good order. Otherwise, if the membrane did not contain any meta-atoms at all, the appearance of the membrane would have been completely transparent. The membrane was rolled into a spherical shape as shown in **Figure 5b**. By adding water, the water dissolvable PVA membrane boundary collapsed and thus reorientation and rearrangement of the meta-atoms started. The membrane itself then served as a host medium for the meta-atoms. Finally, the host medium containing the randomized meta-atoms (RMs) was reshaped to exhibit two plan parallel surfaces, while additionally the water was removed. Further details are given in the Experimental Section. To confirm randomness in orientation

and arrangement of the meta-atoms, a 1.5 μm thick layer of RM was prepared and placed between a conductive silver paint (CSP) and a platinum (Pt) layer improving the electron-microscopical inspection. **Figure 5c** shows a cross-sectional view of the described stack after cutting with a focused ion beam. A magnified view of the RM is displayed in **Figure 5d**, where even the thin dielectric spacer between the metallic layers is noticeable.

For optical inspection, a host medium with RM measuring a thickness of 25 μm sandwiched between a fused silica substrate and an empty host medium slab was prepared. The empty slab is supposed to inhibit Fabry–Perot resonances and does not contain any meta-atom at all, but apart from this it was treated exactly like the host medium with the RM. Details regarding the transparency of the slab can be found in the supporting information. The optical transmittance spectrum of the RM (red line, denoted as “3d”) in comparison to the well-ordered planar arranged nanostructures (blue line, denoted as “2d”) is shown in **Figure 5e**. There are two obvious differences between the two samples. First, the randomized 3d sample shows an overall decreased transmittance. Second, the MDR is slightly blue shifted. The latter can be explained by the angle dependence of the spectral transmission features of

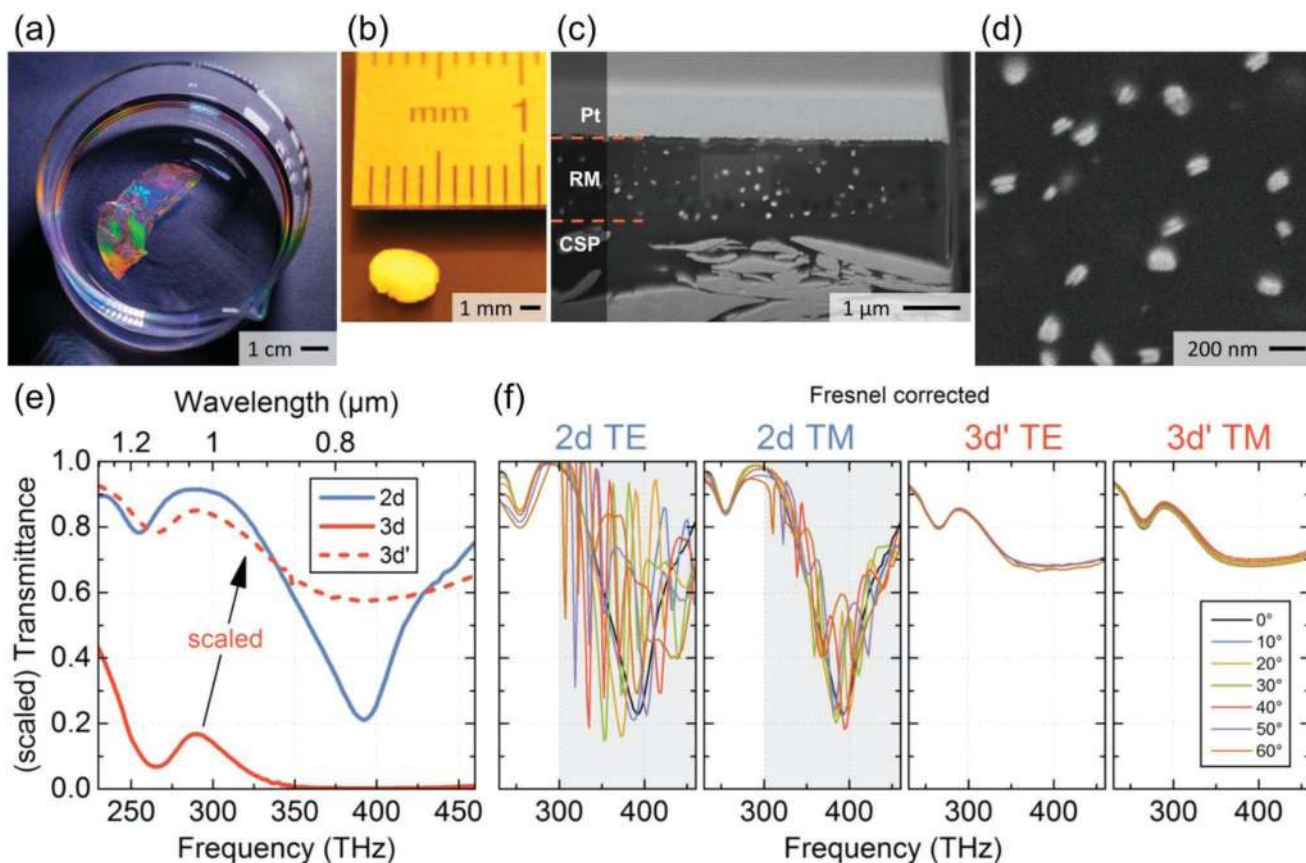


Figure 5. a) Photograph of the meta-atom array containing membrane after peeling off. b) Photograph of the membrane rolled into a spherical shape. c) Cross-sectional SEM image of the 3D photonic nanomaterial. d) Magnified view of (c) to emphasize the meta-atoms being reoriented and rearranged. e) Transmittance spectra comparing the well-ordered planar single layer film (2d), the randomized membrane (3d), and the data of the randomized membrane rescaled to the effective thickness of the single layer (3d'). f) Incident angle dependent transmittance spectra for TE and TM polarization. The gray shaded areas in the 2d-diagrams mark the spectral region, where grating resonances dominate the transmittance spectra.

the meta-atoms, which will be studied further below for the 2d case (see Figure 5f) and which overlay in the randomized 3d arrangement. Additionally, the embedding of the meta-atoms in the 3d arrangement is slightly different from the 2d case in that the high index substrate is removed, which also explains the slight blue shift of the resonance features. The former and most prominent difference, which is the overall decreased transmittance, is due to the 50-fold increase in physical thickness of the randomized 3d film (25 μm) as compared to the 2d planar arrangement (500 nm including the PVA embedding layer) resulting in multiple light-meta-atom interactions when light penetrates through the layer. To allow for a better visual comparison of the two spectra despite their significant thickness difference, the 3d measurement is rescaled to an effective single layer by applying the inverse Lambert-Beer's law, shown by the red dashed line in Figure 5e and denoted as "3d'." Please note, instead of the full factor 50 the factor 10 was applied in this rescaling since the strength of the resonances are supposed to suffer from disorder^[10,35] and the randomized orientation of the meta-atoms leads to decreased excitation efficiency of the resonances.^[36] This rescaled transmittance allows for a detailed comparison between the 2d and 3d cases. While their good correspondence demonstrates the general robustness of the MDR and EDR against positional and orientational disorder, it also reveals a broadening of the resonance due to inhomogeneous multiple meta-atom interactions and multiple path scattering.

Finally, the optical response in transmittance upon varying the incident angle has been analyzed and is shown in Figure 5f. The sample was investigated before ("2d TE/TM", two diagrams on the left) and after ("3d' TE/TM", two diagrams on the right) randomization of the meta-atoms, while the incident angle was changed in steps of 10 degrees and both constellations were illuminated by both TE and TM polarized light respectively. Please note, the displayed graphs include the effective thickness rescaling of the 3d case as described above as well. Also, in all four cases a correction of the angular dependence of Fresnel reflections (R_{fres}) occurring at both planar surfaces limiting the samples has been applied. To compensate for this effect, a correction (T_{corr}) of the measured values (T_{meas}) was done by considering $T_{\text{corr}} = T_{\text{meas}} / (1 - R_{\text{fres}})^2$. Comparing the resulting graphs for 2d and 3d', two major differences become obvious. First, the oblique incidence spectra for the 2d case for frequencies larger than 300 THz (gray shaded spectral regions) show distinct grating resonances superimposing the EDR. This is a clear feature of the ordered lattice of meta-atoms for this case, which is fully suppressed by the positional disorder in the 3d' case. Second, the angular dispersion in the spectra of the 2d case is conspicuous, including also the variation of the resonance width of the MDR, which originates from the optical anisotropy of the metasurface. In contrast, the 3d' sample shows almost negligible angle dependence in both, TE and TM polarization, confirming the optical isotropy of the voluminous meta-material due to orientational disorder of its meta-atoms.

4. Conclusion

In conclusion, by experimental realization the transformation of a subwavelength nanostructured metasurface to a

voluminous photonic nanomaterial was investigated for the first time from a morphological and optical point of view. Departing from a perfect periodically arranged nanostructure array, it was shown that the magnetic and electric dipole resonances of the meta-atoms are preserved even after transforming the metasurface into a voluminous photonic nanomaterial including a randomized orientation and arrangement of the meta-atoms. One key finding is, that, although operating in-plane, well-established nanolithography can be utilized to realize an optically functionalized voluminous photonic nanomaterial. The second key finding is the possible transformation of an optically anisotropic behavior inherently connected with the design of the individual meta-atom or with the arrangement in the metasurface, into an isotropic behavior making the optical response independent from the incident angle of light. The herein presented results relax constraints on concept, design and integration of optical voluminous photonic nanomaterials. Additionally, it should be emphasized that the optically functionalized membrane on the one hand, and the voluminous photonic nanomaterial on the other hand, can be spatially transferred onto any surface with the presented peel-off procedure. In a nutshell, this work paves the way for "photonic nanomaterials available from a paint bucket."

The designed material is understood to be prototypical and only shows exemplarily what is possible. Generally, with the chosen approaches materials with much more complicated and diverse properties could be achieved that may find use in multiple applications. Materials with a strong electric response, for example, could be used as high-index immersion liquids if operated off-resonant, improving with that microscopy techniques. Materials made from chiral meta-atoms could offer a huge circular dichroism that would allow to implement devices that can control the polarization on very short length scales. Also, bulky materials with either a strong electric or magnetic resonance could tailor the emission properties of quantum emitters brought in close proximity that is beneficial for lightning devices. There are plenty of options along these lines with materials made with the approach detailed in this contribution.

5. Experimental Section

Realization of Meta-Atoms: For the nanostructure realization the following initial layer stack was set up: Onto a circular 100 mm diameter fused silica wafer, a 500 nm thin layer of AZ 1505 from MicroChemicals was applied by spin-coating, followed by a post apply bake at 200 °C for 30 min. Subsequently, 200 nm of electron-beam resist AR-P 617 and 100 nm of AR-P 6200, both from Allresist, were spun-on and tempered at 200 °C for 10 min and 150 °C for 3 min, respectively. The nanostructure was defined by electron beam lithography in cell projection mode by means of an electron-beam writing tool SB 350-OS from Vistec. The exposed layer stack was developed first by AR 600-54/6 for 30 s and second by a mixture of MIBK and isopropanol with a volume ratio of 1:1 for 80 s. The resist mask was transferred into the final functional nanostructure pattern by applying shadow evaporation followed by lift-off in an acetone bath for several hours. The evaporation took place in a self-assembled electron beam induced physical vapor deposition chamber, where source and substrate were about 60 cm apart. The evaporated layer stack thicknesses were controlled in situ by a quartz

crystal oscillator. Prior a 3 nm titanium layer for an increased adhesion between Au and AZ 1505 was evaporated.

Realization of Isotropic 3D Photonic Nanomaterial: The meta-atoms on the wafer were spin-coated by a mixture of polyvinyl alcohol (PVA) from Sigma-Aldrich and purified water with a weight ration of 1:10, while after heating at 100 °C for 5 min a thickness of 500 nm PVA remained on the surface. The wafer was immersed in heated AZ-Remover at 70 °C for several hours to peel-off the PVA membrane along with the nanostructures. The peeled-off membrane was rinsed in acetone and isopropanol and rolled manually into a spherical shaped cluster after dry blowing. Then pure water was added to the cluster. The aggregate was compacted by two plane parallel plates and simultaneously gently heated to 40 °C.

Investigation: The morphology of the nanostructure was investigated by both, a scanning electron beam microscope S-4800 from Hitachi and a dual beam Neon 60 from Zeiss. Optical performances of the different samples were investigated by a spectral photometer Lambda 950 from Perkin Elmer and a self-constructed angle resolved spectral photometer. The transmitted light was detected by either a photomultiplier or a polycrystalline lead sulfide detector mounted on an integration sphere.

Numerical Analysis: Numerical simulations were accomplished with the software package FDTD Solutions from Lumerical Inc. The optical properties of the used materials were either adopted from^[37] for Au and^[38] for fused SiO₂ or measured by ellipsometry for PVA. The modeled elementary cell was 400 nm in width. For the calculation of the scattering cross section, perfectly matching layers were applied. In contrast, to obtain the transmittance spectrum of an array of meta-atoms, periodic boundary conditions in *x*- and *y*-directions were applied. The early shutoff criterion was set to 10⁻⁶. The mesh spacing was set to 2 nm in lateral and 1 nm in vertical direction.

Supporting Information

Supporting Information is available from the Wiley Online Library or from the author.

Acknowledgements

The authors acknowledge support by the German Research Foundation in the project MetaLiquid (KL 1199/6-1, RO 3640/3-1, and PE 1524/7-1), in the priority program SPP 1839 Tailored Disorder (PE 1524/10-2, RO 3640/7-2 under project number 278747906), and from the Excellence Cluster 3D Matter Made to Order (EXC 2082/1 under project number 390761711), as well as by the German Federal Ministry of Education and Research (03ZZ0451 and 03Z1H534). The authors thank Oliver Puffky, Christoph Menzel, Jan Sperrhake, and Martin Fruhnert for their constructive comments and suggestions.

Conflict of Interest

The authors declare no conflict of interest.

Author Contributions

K.D., T.P., C.R., A.T., and E.-B.K. conceived and designed the experiment. K.D., T.S., M.S., and U.H. fabricated all samples and prepared and analyzed the SEM inspections. K.D. and M.Z. performed the optical inspections. K.D. performed the numerical investigation. K.D., C.R., and T.P. wrote the manuscript, and all authors contributed to the final version.

Keywords

artificial photonic nanomaterial, cut-wire-pair, electron-beam lithography, optically isotropic material, self-assembly

Received: July 15, 2019
Revised: October 14, 2019
Published online:

- [1] N. I. Zheludev, Y. S. Kivshar, *Nat. Mater.* **2012**, *11*, 917.
- [2] N. Meinzer, W. L. Barnes, I. R. Hooper, *Nat. Photonics* **2014**, *8*, 889.
- [3] C. M. Soukoulis, M. Wegener, *Science* **2010**, *330*, 1633.
- [4] M. Kadic, G. W. Milton, M. van Hecke, M. Wegener, *Nat. Rev. Phys.* **2019**, *1*, 198.
- [5] N. J. Halas, *Nano Lett.* **2010**, *10*, 3816.
- [6] F. von Cube, S. Irsen, R. Diehl, J. Niegemann, K. Busch, S. Linden, *Nano Lett.* **2013**, *13*, 703.
- [7] M. Esposito, V. Tasco, F. Todisco, M. Cuscunà, A. Benedetti, M. Scuderi, G. Nicotra, A. Passaseo, *Nano Lett.* **2016**, *16*, 5823.
- [8] P. L. Madhuri, R. J. Martín-Palma, B. Martín-Adrados, I. Abdulhalim, *J. Mol. Liq.* **2019**, *281*, 108.
- [9] I. Abdulhalim, P. L. Madhuri, M. Diab, T. Mokari, *Opt. Express* **2019**, *27*, 17387.
- [10] C. Helgert, C. Menzel, C. Rockstuhl, E. Pshenay-Severin, E.-B. Kley, A. Chipouline, A. Tünnermann, F. Lederer, T. Pertsch, *Opt. Lett.* **2009**, *34*, 704.
- [11] M. Hentschel, M. Schäferling, T. Weiss, N. Liu, H. Giessen, *Nano Lett.* **2012**, *12*, 2542.
- [12] W. S. Chang, J. B. Lassiter, P. Swanglap, H. Sobhani, S. Khatua, P. Nordlander, N. J. Halas, S. Link, *Nano Lett.* **2012**, *12*, 4977.
- [13] M. Semmlinger, M. L. Tseng, J. Yang, M. Zhang, C. Zhang, W. Y. Tsai, D. P. Tsai, P. Nordlander, N. J. Halas, *Nano Lett.* **2018**, *18*, 5738.
- [14] D. B. Burckel, J. R. Wendt, G. A. Ten Eyck, J. C. Ginn, A. R. Ellis, I. Brener, M. B. Sinclair, *Adv. Mater.* **2010**, *22*, 5053.
- [15] Y. Zhao, M. A. Belkin, A. Alù, *Nat. Commun.* **2012**, *3*, 870.
- [16] M. Jang, Y. Horie, A. Shibukawa, J. Brake, Y. Liu, S. M. Kamali, A. Arbabi, H. Ruan, A. Faraon, C. Yang, *Nat. Photonics* **2018**, *12*, 84.
- [17] C. Helgert, C. Rockstuhl, C. Etrich, C. Menzel, E.-B. Kley, A. Tünnermann, F. Lederer, T. Pertsch, *Phys. Rev. B* **2009**, *79*, 233107.
- [18] S. Fasold, S. Linß, T. Kawde, M. Falkner, M. Decker, T. Pertsch, I. Staude, *ACS Photonics* **2018**, *5*, 1773.
- [19] J. A. Fan, V. N. Manoharan, N. J. Halas, R. Bardhan, P. Nordlander, C. Wu, J. Bao, G. Shvets, K. Bao, F. Capasso, *Science* **2010**, *328*, 1135.
- [20] V. Ponsinet, P. Barois, S. M. Gali, P. Richetti, J. B. Salmon, A. Vallecchi, M. Albani, A. Le Beulze, S. Gomez-Grana, E. Duguet, S. Mornet, M. Treguer-Delapierre, *Phys. Rev. B* **2015**, *92*, 220414.
- [21] C. Rockstuhl, T. Scharf, *Amorphous Nanophotonics*, Springer, Berlin, **2013**.
- [22] B. Kante, K. O'Brien, A. Niv, X. Yin, X. Zhang, *Phys. Rev. B* **2012**, *85*, 041103.
- [23] W. Lewandowski, M. Fruhnert, J. Mieczkowski, C. Rockstuhl, E. Górecka, *Nat. Commun.* **2015**, *6*, 6590.
- [24] Z. Qian, S. P. Hastings, C. Li, B. Edward, C. K. McGinn, N. Engheta, Z. Fakhraai, S. J. Park, *ACS Nano* **2015**, *9*, 1263.
- [25] R. Verre, N. O. Länk, D. Andrén, H. Šípová, M. Käll, *Adv. Opt. Mater.* **2018**, *6*, 1701253.
- [26] R. Verre, L. Shao, N. O. Länk, P. Karpinski, A. B. Yankovich, T. J. Antosiewicz, E. Olsson, M. Käll, *Adv. Mater.* **2017**, *29*, 1701352.
- [27] X. Shen, A. Asenjo-Garcia, Q. Liu, Q. Jiang, F. J. García de Abajo, N. Liu, B. Ding, *Nano Lett.* **2013**, *13*, 2128.

- [28] A. Kuzyk, R. Schreiber, H. Zhang, A. O. Govorov, T. Liedl, N. Liu, *Nat. Mater.* **2014**, *13*, 862.
- [29] S. Gomez-Graña, A. Le Beulze, M. Treguer-Delapierre, S. Mornet, E. Duguet, E. Grana, E. Cloutet, G. Hadziioannou, J. Leng, J. B. Salmon, V. G. Kravets, A. N. Grigorenko, N. A. Peyyety, V. Ponsinet, P. Richetti, A. Baron, D. Torrent, P. Barois, *Mater. Horiz.* **2016**, *3*, 596.
- [30] E.-B. Kley, H. Schmidt, U. Zeitner, M. Banasch, B. Schnabel, *Proc. SPIE* **2012**, *8352*, 83520M.
- [31] U. Hübner, M. Falkner, U. Zeitner, M. Banasch, K. Dietrich, E.-B. Kley, *Proc. SPIE* **2014**, *9231*, 92310E.
- [32] N. Liu, H. Guo, L. Fu, S. Kaiser, H. Schweizer, H. Giessen, *Adv. Mater.* **2007**, *19*, 3628.
- [33] K. Dietrich, C. Menzel, D. Lehr, O. Puffky, U. Hübner, T. Pertsch, A. Tünnermann, E.-B. Kley, *Appl. Phys. Lett.* **2014**, *104*, 193107.
- [34] P. Hudek, U. Denker, D. Beyer, N. Belic, H. Eisenmann, *Microelectron. Eng.* **2007**, *84*, 814.
- [35] M. Albooyeh, S. Kruk, C. Menzel, C. Helgert, M. Kroll, A. Krysinski, M. Decker, D. N. Neshev, T. Pertsch, C. Etrich, C. Rockstuhl, S. A. Tretyakov, C. R. Simovski, Y. S. Kivshar, *Sci. Rep.* **2015**, *4*, 4484.
- [36] M. Y. Sushko, *J. Phys. D: Appl. Phys.* **2009**, *42*, 155410.
- [37] P. Johnson, R. Christy, *Phys. Rev. B* **1974**, *9*, 5056.
- [38] I. H. Malitson, *J. Opt. Soc. Am.* **1965**, *55*, 1205.